JLAB-TN-01-025

Hall A HRS Acceptance Study via White Spectrum Scans in Experiment E94-004

Paul E. Ulmer

Department of Physics
Old Dominion University
Norfolk, VA 23529-0116

May 22, 2001

Abstract: Relative acceptance profiles for the Hall A electron (*i.e.* "left") and hadron (*i.e.* "right") spectrometers were obtained during a three day E94-004 run in October of 1999 (as a calibration for the d$(e, e'p)$n cross section measurements). The deconvolution of acceptance and physics cross section was accomplished by applying a fitting technique to a series of white spectrum scans. The scans were performed by varying the magnetic fields of each spectrometer by 2% per measurement for each of five measurements (for a total of roughly 10%, comparable to the spectrometer's momentum acceptance). The scans for the two spectrometers were done in parallel by acquiring prescaled data on each. Simulations based on MCEEP with the magnetic/aperture model of J. LeRose give reasonable agreement with the shapes extracted from data especially if the radius of Q3 is reduced from 0.30 m to 0.28 m.

Contents

1 Introduction

Knowledge of the spectrometer/detector acceptance-efficiency product is often one of the dominant sources of uncertainty in extracting cross sections. For the Hall A high resolution spectrometers (HRS), the acceptance is normally defined by a combination of front-end slits (for this study, the nominally 6.0 msr collimators were used) and subsequent magnet apertures. As the magnet apertures partially define the acceptance, the magnetic model must be known in order to predict the acceptance function. This makes the determination of acceptance complicated and it is essential that model predictions be checked against data. In addition, variation of the detector efficiencies can distort the "acceptance function". However, provided the detector thresholds and high voltages have been properly adjusted, the efficiencies are expected to be nearly 100% across the acceptance, so that this latter effect can usually be neglected. In that case, since the detectors are not expected to be acceptance limiters, a measure of the acceptance/efficiency product is primarily a measure of the spectrometer acceptance function.

One can determine the spectrometer acceptance by populating it fully (*i.e.* oversampling) and examining whether particular combinations of (Transport variables [1]) x_t, θ_t, y_t, ϕ_t and δ_t are present in the data. (Here, the subscript t indicates quantities traced back to the target, though one can use any location in the spectrometer, in principle, to define this set of coordinates since they uniquely determine the ray followed by a particle.) The result would be a "logical map" (*i.e.* a "yes/no" map defining whether a given combination of coordinates is within the acceptance) over this five-dimensional phase space. For a reasonably fine mesh, such a map would require a very large statistical sample (and, consequently, a large amount of beam time). Therefore, one usually integrates over some set of variables to extract the acceptance profile as a function of the others. The integration has two drawbacks. The obvious drawback is that one loses complete information about the acceptance function. The other is that any measurement involves a cross section which varies over the acceptance. Thus, it is not valid to use the number of counts in a given channel to define the "relative" acceptance profile (*i.e.* the acceptance of this channel relative to some reference channel), as the yield reflects the integral of the **cross section weighted** phase space. Therefore, one must deconvolute cross section and acceptance in the yield spectrum. This is the purpose of the present technique.

By selecting kinematics with a cross section which is nearly uniform across the acceptance, one minimizes the effect of this dependence on extracting the acceptance function. Further, by scanning the cross section across the acceptance in small, overlapping steps, one can fit its functional dependence since a given "channel" of the spectrometer will sample different cross sections. Since the cross section depends on momentum and angle, the scan should be performed over a two-dimensional grid. Given the limitations of beam time for this experiment (three calendar days to acquire all the calibrations and data), a one-dimensional scan in δ was performed at fixed spectrometer angle. The resulting "acceptance" profiles then involve an integral over the angular dependence of the cross section for a given momentum. Given the angular dependence is not too extreme, the result will be close to the actual acceptance profile.

2 The Technique

The computer code of H. Baghaei [2], subsequently modified by J. Gao [3] and this author was used to deconvolute the acceptance/efficiency profile from the physics cross section momentum dependence. The technique is described in several theses from MIT/Bates (see [2] for example), and is repeated here for completeness.

The shape of the spectrum *vs.* momentum is fit with an n^{th} order polynomial (here, taken to be a fourth order Legendre polynomial). The predicted number of counts in channel i for the k^{th} measurement is:

$$C_{ik}^{th} = \sigma_{ik} N_k \epsilon_i$$

where σ_{ik} is the cross section for channel i and measurement k and is approximated by

$$\sigma_{ik} = \sum_{l=0}^{n} A_l P_l(p_{ik})$$

where P_l is the l^{th} order Legendre polynomial. N_k is the normalization factor for run k, ϵ_i is the relative acceptance/efficiency of channel i and p_{ik} is the momentum sampled by channel i for measurement k. An iterative procedure is used to determine both the coefficients, A_l, and the relative "efficiencies". The coefficients are determined by minimizing χ^2:

$$\chi^2 = \sum_{i,k} \left(C_{ik}^{ex} - C_{ik}^{th} \right)^2 w_{ik}$$

where C_{ik}^{ex} is the measured number of counts for channel i and measurement k and w_{ik} is a statistical weighting factor. Since the ϵ_i have not yet been determined, they are all set to unity for the first pass. By minimizing χ^2 for the coefficients:

$$\frac{\partial \chi^2}{\partial A_m} = 0$$

we get a system of linear equations:

$$X_m = \sum_{l=0}^{n} M_{ml} A_l$$

where

$$X_m = \sum_{i,k} C_{ik}^{ex} w_{ik} N_k \epsilon_i P_m(p_{ik})$$

and

$$M_{ml} = \sum_{i,k} (N_k \epsilon_i)^2 w_{ik} P_m(p_{ik}) P_l(p_{ik}).$$

The coefficients are then found by inverting the matrix, M: $A = M^{-1}X$. The relative "efficiencies" can be computed by comparing the predicted number of counts, C^{th}, to the measured number, C^{ex}:

$$\epsilon_i = \frac{\sum_k C_{ik}^{ex}}{\sum_k N_k \sum_{l=0}^{n} A_l P_l(p_{ik})}.$$

A new χ^2 is computed with these efficiencies and new coefficients, A_l, are determined. The procedure is repeated until convergence is established for both the coefficients and the relative efficiencies. Here, convergence was taken to mean a change of less than 10% in χ^2.

This technique does not determine the absolute acceptance-efficiency product, but rather this product for each channel relative to some reference channel. Absolute normalizations (on hydrogen) are used to establish the absolute scale. Here, the acceptance/efficiency profile is scaled to give an average of unity (per momentum channel) over the fitting interval. The resulting profile reflects the integral of detection efficiency for a given momentum channel over the acceptance feeding that channel. The deviation from an ideal flat curve is due mostly to acceptance variations as the detection efficiency is expected to be close to 100%.

3 Experimental Details

The kinematics were: $e = 3.109$ GeV, $\theta_e = 16.057°$, $\theta_p = -76.721°$ for the beam energy, electron arm and hadron arm central angles, respectively. The momentum for the electron arm was varied between 0.954 GeV/c and 1.033 GeV/c in five uniformly spaced steps. The momentum for the hadron arm was varied between 0.823 GeV/c and 0.759 GeV/c in five uniformly spaced steps. The spectrometer angles were kept fixed throughout this study. The target was a 15 cm LD_2 cell.

The trigger rates varied from 0.13 MHz to 0.086 MHz for the electron arm and from 940 Hz to 1300 Hz for the hadron arm with beam currents of 10–15 μA. The electron prescale was set to 100:1 and the hadron to 1:1 so that the T1 and T3 trigger rates were comparable. Small corrections for target density were made based on a target boiling study. Electronic deadtime (for the electron arm only - the hadron arm electronic deadtime was neglected given the relatively low rate) was estimated from the production $d(e,e'p)n$ runs (where the electron kinematics were fixed and the beam current varied strongly over the measured kinematic range) after backing out the effect from target density. (The target density variation was determined from a boiling study in which both spectrometers were fixed and the proton spectrometer rate was always low - thus, the dependence of proton rate on beam current was taken to be a measure of the target density variation.) The electronic deadtime corrections for these acceptance/efficiency scans were estimated to be:

$$d_{EDT-e} = 1 + \frac{0.0012}{\mu\mathrm{A}}\, I$$

$$d_{EDT-h} = 1$$

where I is the beam current. The target density was estimated to follow the linear form:

$$\rho_{corr} = 0.167\mathrm{g/cm}^3 \left(1 - \frac{0.0011}{\mu\mathrm{A}}\, I\right).$$

The yield spectra *vs.* δ were corrected accordingly and the acceptance profiles extracted by the method outlined above.

4 MCEEP Study

To the extent that the relative acceptance/efficiency profile reflects acceptance variations versus δ, it can be modeled using MCEEP [4] which incorporates the magnetic/aperture model of J. LeRose [5]. Only the ratio between the data and MCEEP profiles should then be applied as a correction to data, since MCEEP is used to acceptance average the theory and to determine the experimental two-spectrometer phase space.

The MCEEP extraction of the relative acceptance/efficiency profile is far simpler than for the data since the cross section can be "turned off" (set to unity). The resulting distribution is phase space only and reflects the variation of acceptance versus δ.

5 Results

For each spectrometer, there was one complication in extracting the acceptance/efficiency profile due to contamination by events with distributions not entirely defined by the usual apertures.

For the electron arm, it was observed that the transverse coordinate at the target (y_t) gives the expected distribution for the 15 cm target cell but superimposed on a significantly wider background. The estimated fraction of counts in the tails of this secondary distribution is consistent with the fraction of pions which would decay in the 23 m spectrometer flight path. The secondary distribution is removed after application of the gas Čerenkov cuts. This can be seen in Figure 1 which shows the y distribution at the target without (top) and with (bottom) the Čerenkov cut for one of the runs. The other reconstructed quantities are shown on both linear (Figure 2) and logarithmic (Figure 3) scales, without (solid) and with (dashed) the Čerenkov cut. The acceptance/efficiency profile was generated for events which pass and fail this cut (note that the sum of these two event classes corresponds to events "without" the cut, as referred to above) and, at least for the case of no further cuts in acceptance, they agree well, as can be seen from Figure 4. In any case, the Čerenkov cut was applied for all the profiles shown below.

For the hadron arm, there was significant background due to events which appear to penetrate the 6.0 msr slit. Events reconstructed to the target were subsequently traced forward to the location of the slit. Cuts on the positional coordinates were then applied to define events which go through the aperture. The cut position was obtained empirically by finding the transition region between high and low density of events. This corresponded roughly with the expected aperture location. The reconstructed quantities at the target are shown for one of the runs without (solid) and with (dashed) this slit cut on linear (Figure 5) and logarithmic (Figure 6) scales. The profiles for events which passed and for events which failed this cut (note that the sum of these two event classes corresponds to events "without" the cut, as referred to above) look markedly different. The results are shown for the case of no further acceptance cuts in Figure 7. All profiles shown below were therefore generated from events which satisfied this slit cut.

An acceptance study was performed by generating separate profiles for a variety of cuts in ϕ, θ and y at the target. Due to the forward electron angle, y cuts only begin

to take effect within the range of ± 2 cm. The hadron arm, however, has the transverse acceptance completely filled.

The results for the data for no acceptance cuts (other than the slit cut referred to above for the hadron arm) are compared to MCEEP in Figure 8 for the electron arm and in Figure 9 for the hadron arm. The agreement is reasonable (though, by no means perfect) except that the data sees a smaller range of δ than predicted. A MCEEP study was performed in which the sizes of the dipole and Q3 apertures were varied to improve agreement. Varying the dipole aperture has little effect, except for unreasonably extreme variations. The results are quite sensitive to the radius of Q3, however. The data are shown *vs.* MCEEP for a radius of 0.28 m (at both entrance and exit of Q3) instead of the actual 0.30 m in Figure 10 and Figure 11. Presumably, though artificial, such a reduction may compensate for inadequacies of the magnetic model. There is a roughly 7% loss in phase space per spectrometer for this reduced radius.

The results for data as a function of various acceptance cuts are shown in Figures 12–14 for the electron arm and in Figures 15–17 for the hadron arm. It can be seen that the shapes for the two arms begin to resemble each other when the vertex cuts are applied, as expected.

6 Summary/Conclusions

The acceptance profiles *vs.* δ have been extracted for the electron arm (now "left" spectrometer) and hadron arm (now "right" spectrometer). The electron arm viewed the 15 cm target cell at a forward angle and so did not have the transverse acceptance completely filled. It shows a fairly flat acceptance profile. On the contrary, the hadron arm which viewed the target at a large angle and therefore had the tranverse acceptance filled shows significant slope for the acceptance profile. This slope is seen in both data and MCEEP (though the MCEEP slope is slightly smaller). If the dipole apertures in MCEEP are turned off, the spectrum becomes flat. If the dipole apertures are enforced, but the index is turned off (*i.e.* the trapezoidal shape becomes a rectangle) the slope persists and, in fact, shows little difference from the result with the actual dipole apertures. The results are quite insensitive to the shape and size of the dipole aperture within reasonable limits but are sensitive to the assumed radius of Q3. Optimal results are achieved for a radius of Q3 of roughly 0.28 m compared with the actual 0.30 m. This reduction leads to about 7% loss in phase space per arm.

Since the cross section has both momentum and angle dependence, this scan does not completely decouple physics from acceptance/efficiency. A two-dimensional (momentum and angle) scan was performed in April 2001. These data are now being analyzed and should determine the HRS acceptance profiles more definitively.

7 Acknowledgments

I thank John LeRose for useful discussions, especially the suggestion of reducing the Q3 radius, and for proofreading this paper.

References

[1] K.L. Brown, F. Rothacher, D.C. Carey and C.H. Iselin, TRANSPORT, *A Computer Program for Designing Charged Particle Beam Transport Systems*, SLAC-91, Rev. 2, UC-28(1/A).

[2] H. Baghaei, MIT Ph.D. thesis (1987).

[3] J. Gao, private communication (2001).

[4] P.E. Ulmer, computer program MCEEP, *Monte Carlo for* $(e, e'p)$ *Experiments*, CEBAF Technical Note # 91-101 (1991).

[5] J. LeRose, private communications.

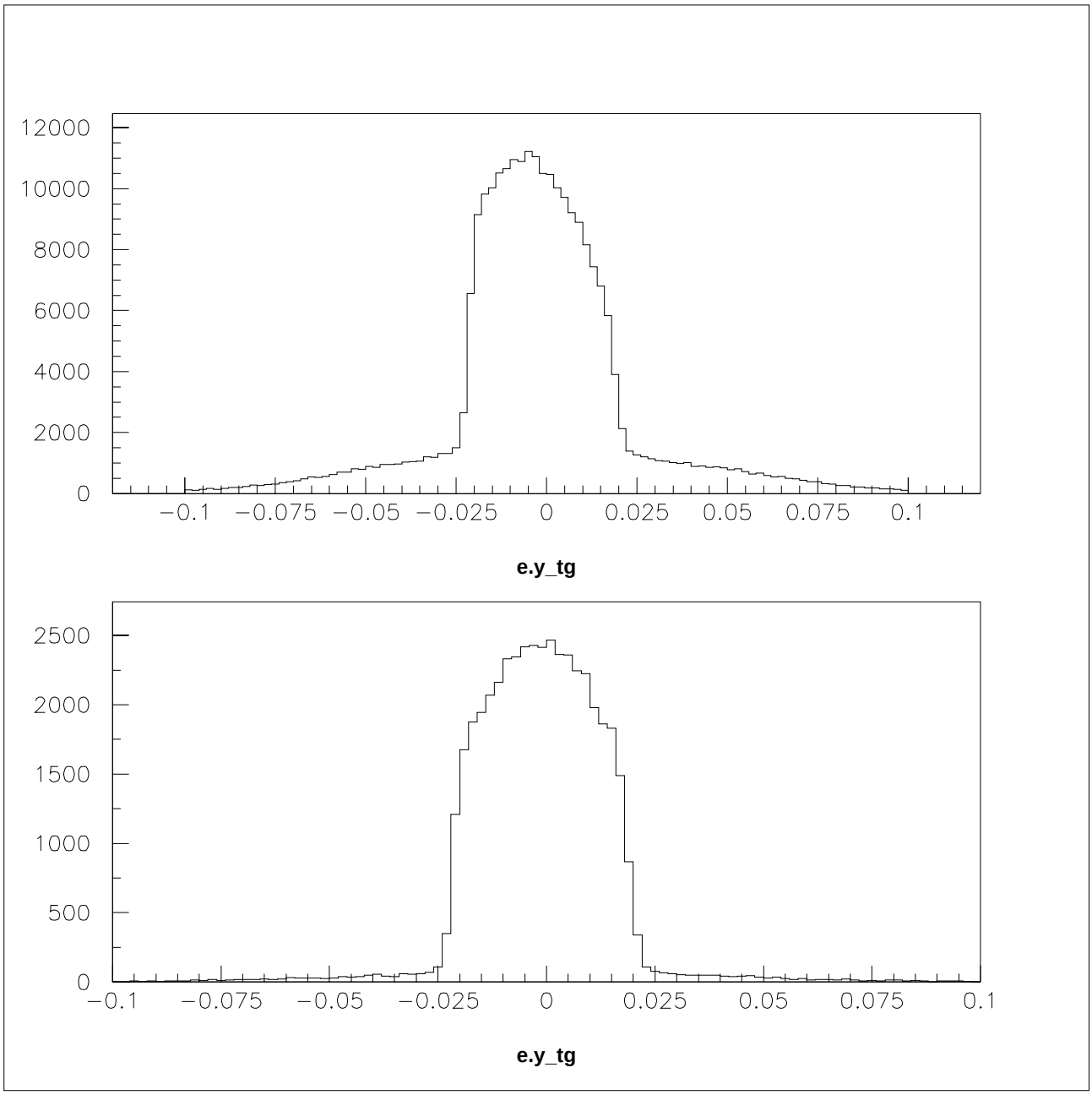

Figure 1: Electron arm y at the target without (top) and with (bottom) the Čerenkov counter cut for one of the runs.

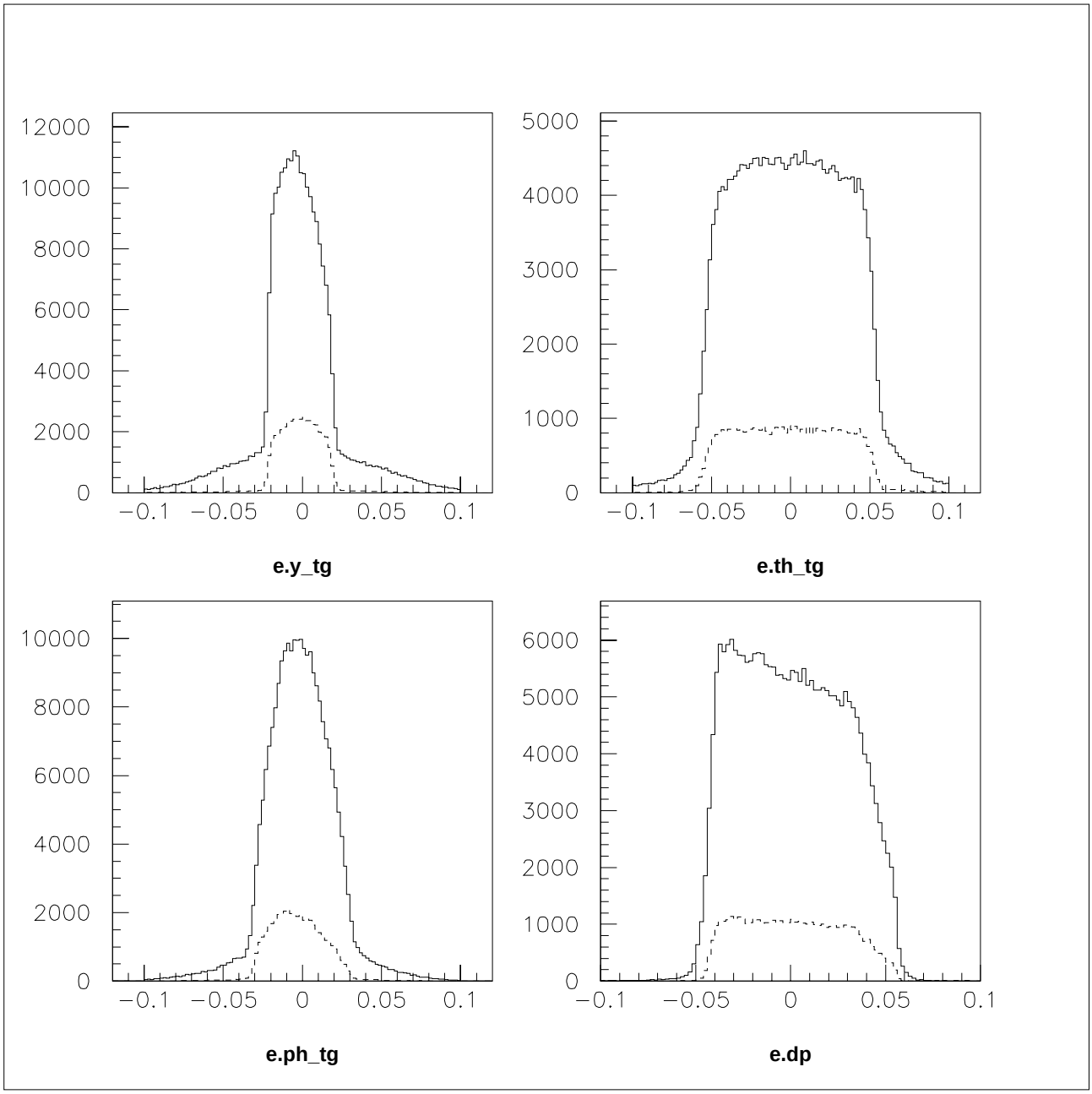

Figure 2: Electron arm reconstructed quantities at the target without (solid) and with (dashed) the Čerenkov counter cut for one of the runs.

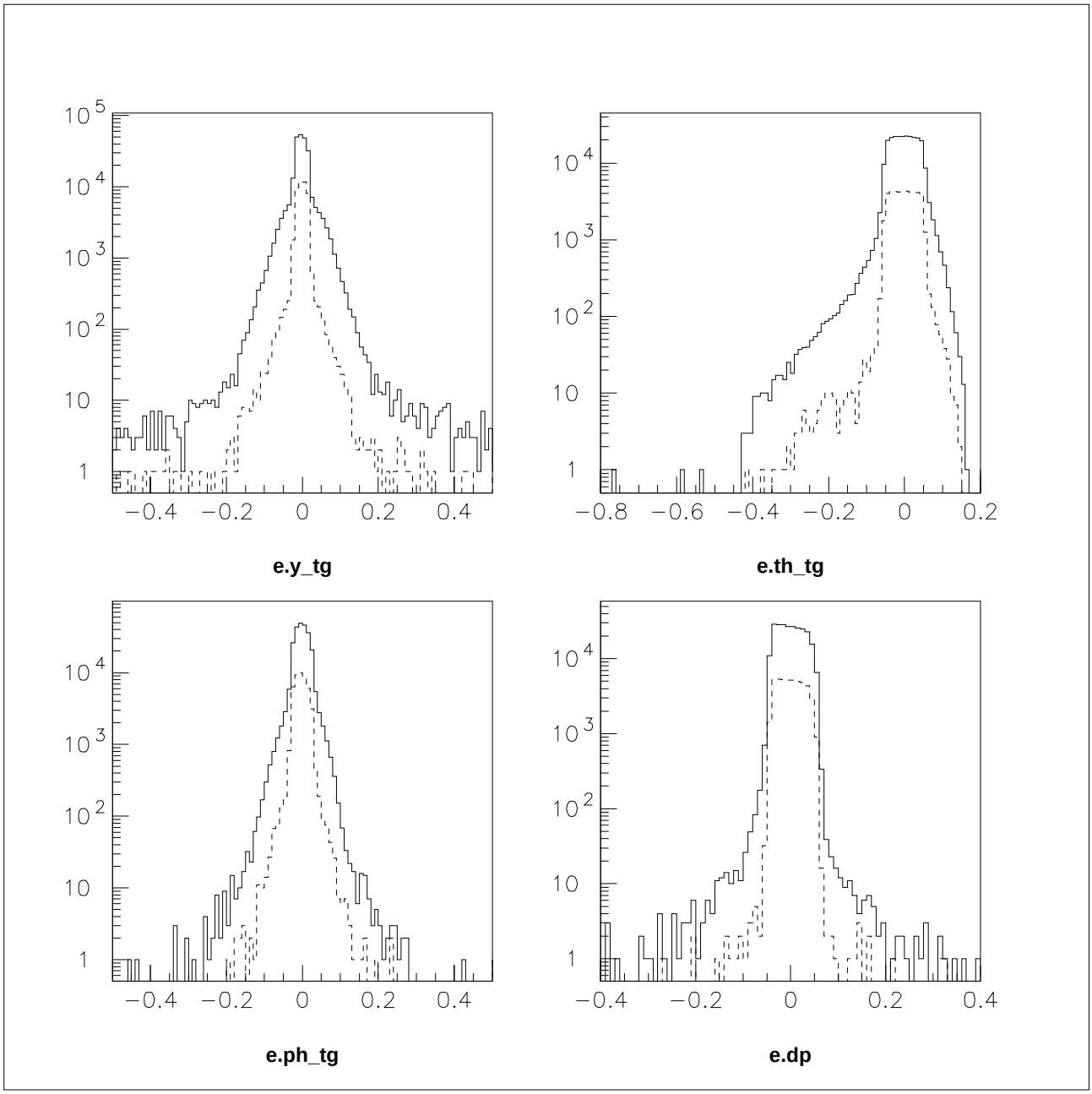

Figure 3: Same as Figure 2 except on a logarithmic scale and with expanded x-axes.

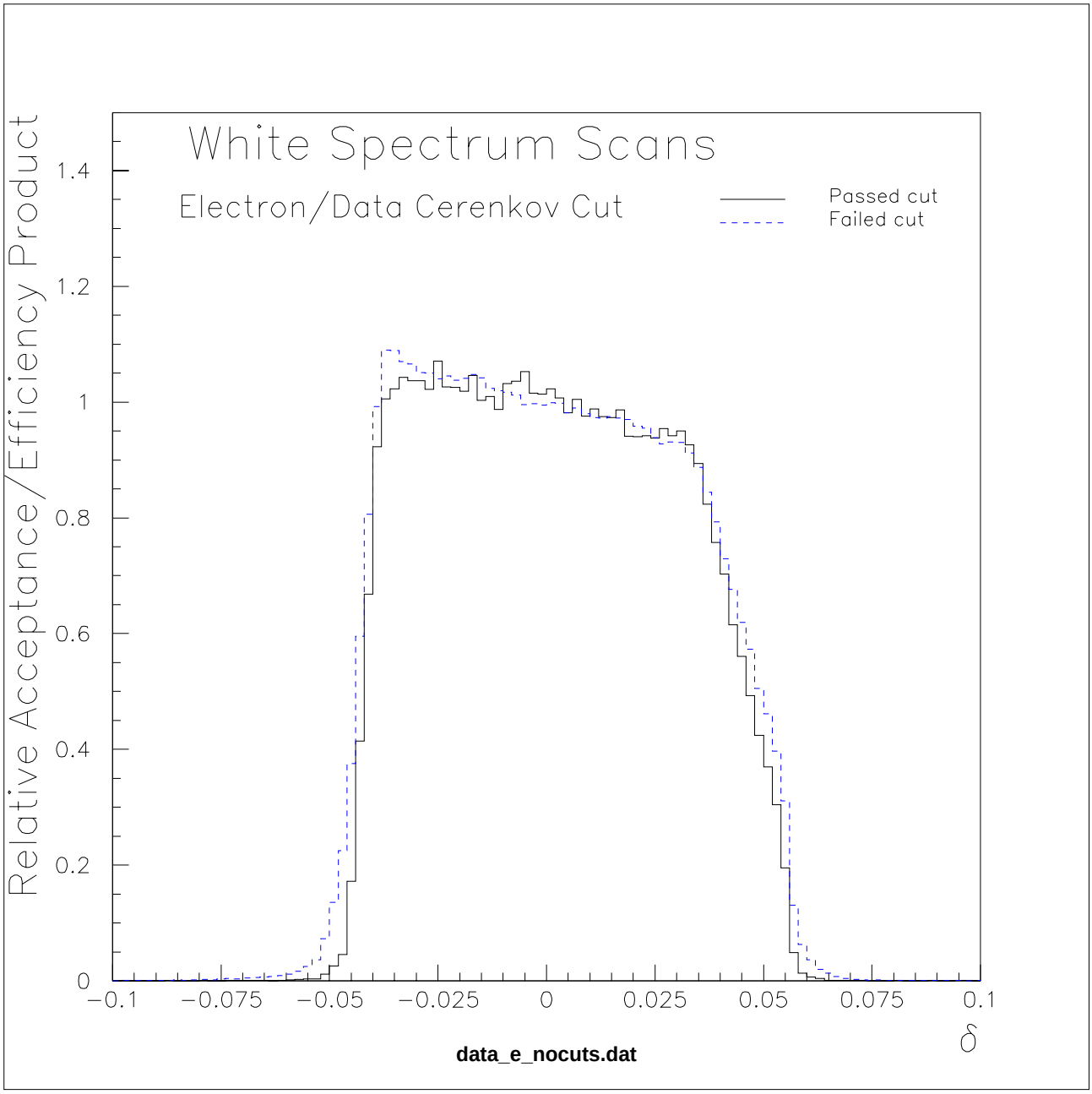

Figure 4: Electron arm relative acceptance/efficiency profile for events which pass and fail the Čerenkov counter cuts. The sum of these two event classes corresponds to "without" the cut in Figures 1–3.

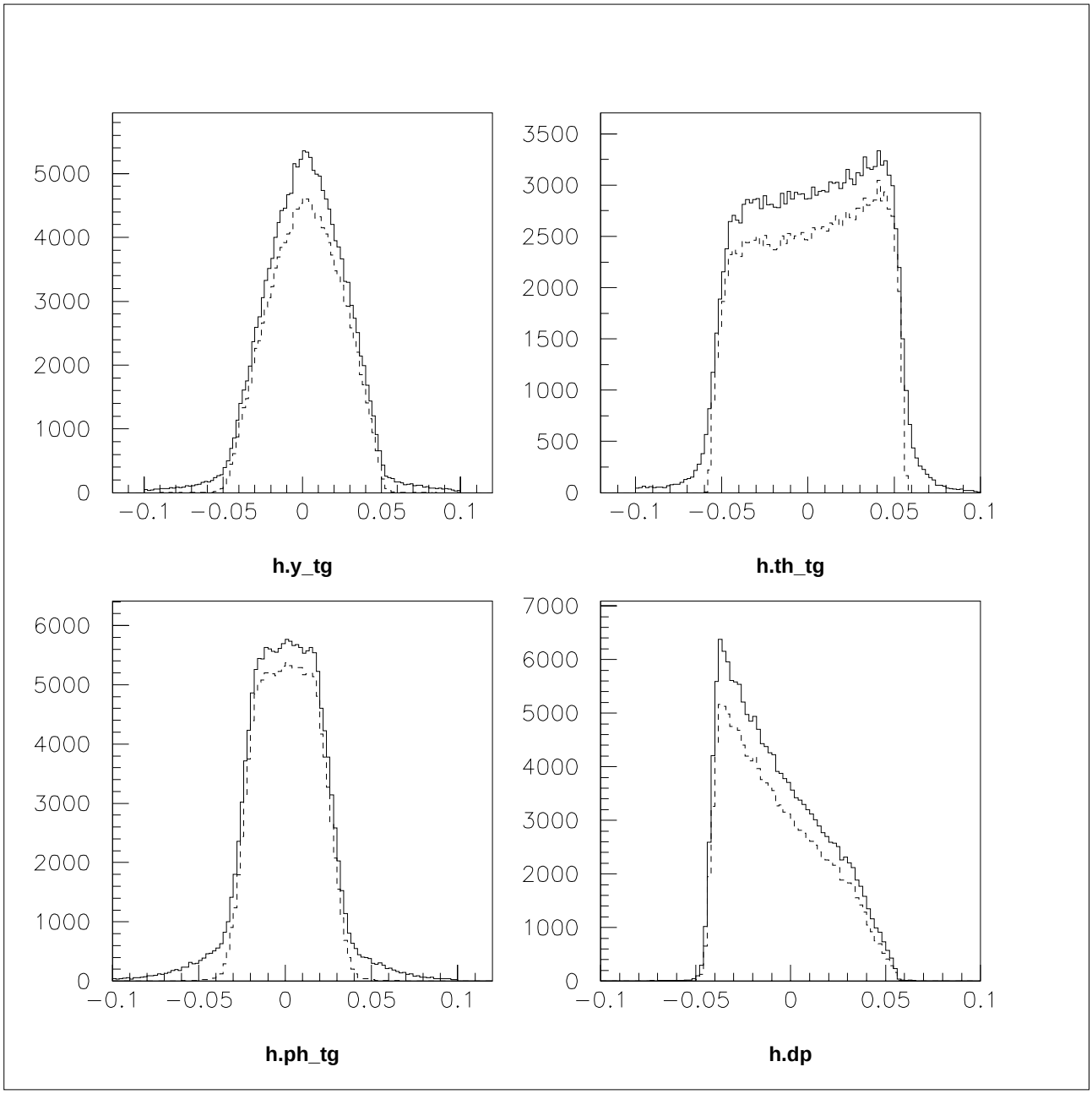

Figure 5: Hadron arm reconstructed quantities at the target without (solid) and with (dashed) the slit cut for one of the runs.

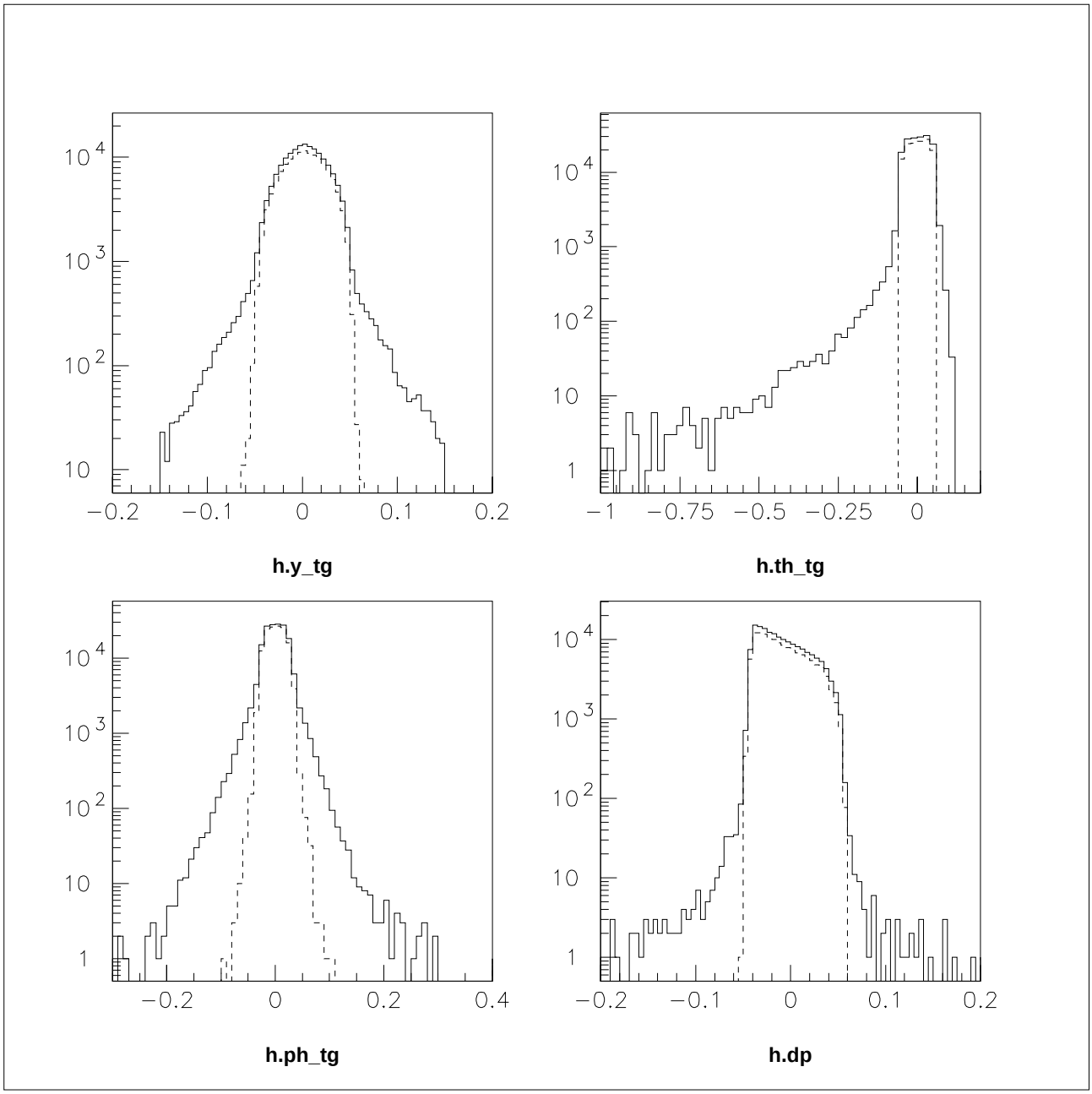

Figure 6: Same as Figure 5 except on a logarithmic scale and with expanded x-axes.

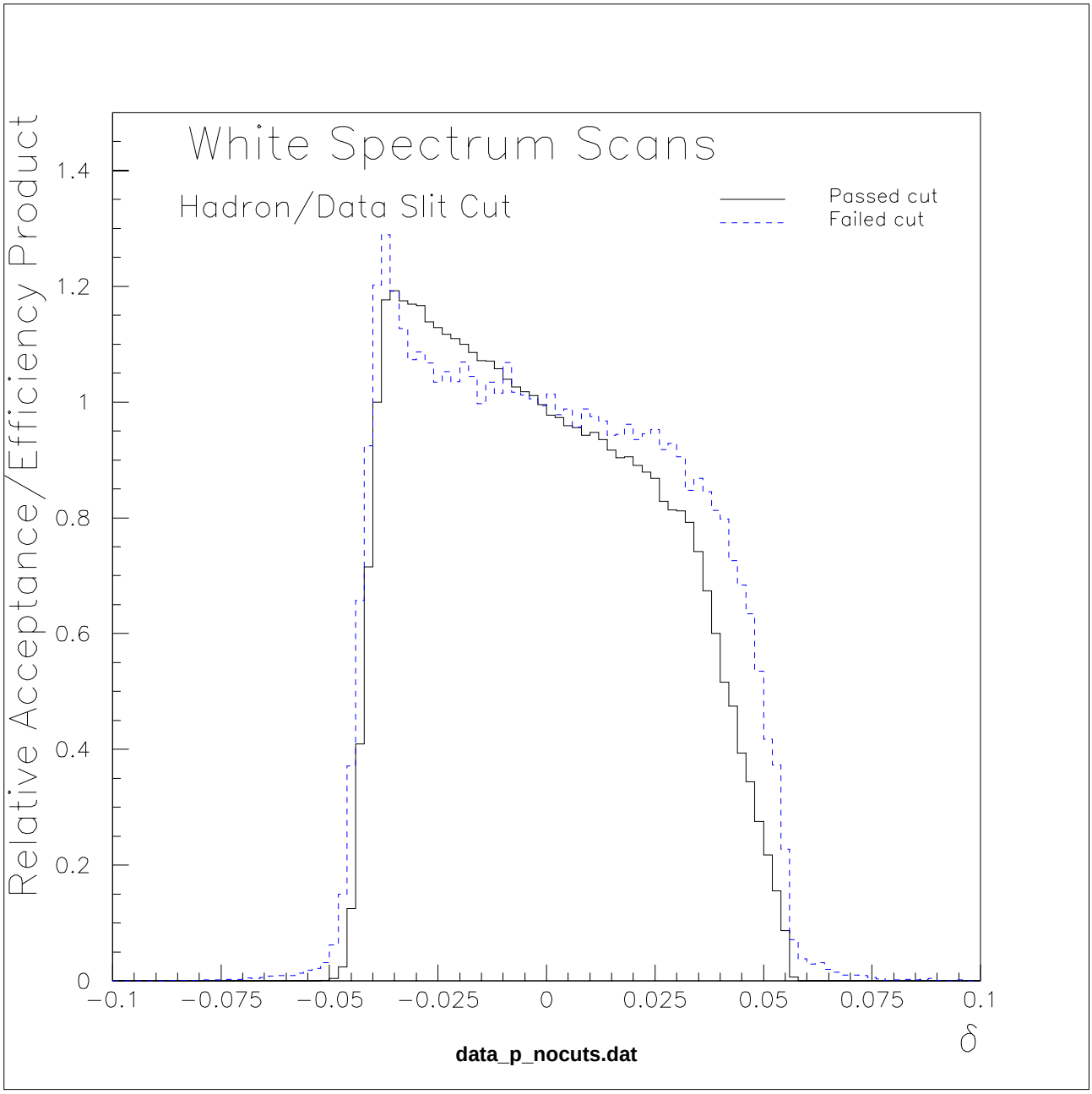

Figure 7: Hadron arm relative acceptance/efficiency profile for events which pass and fail the 6.0 msr slit cut. The sum of these two event classes corresponds to "without" the cut in Figures 5–6.

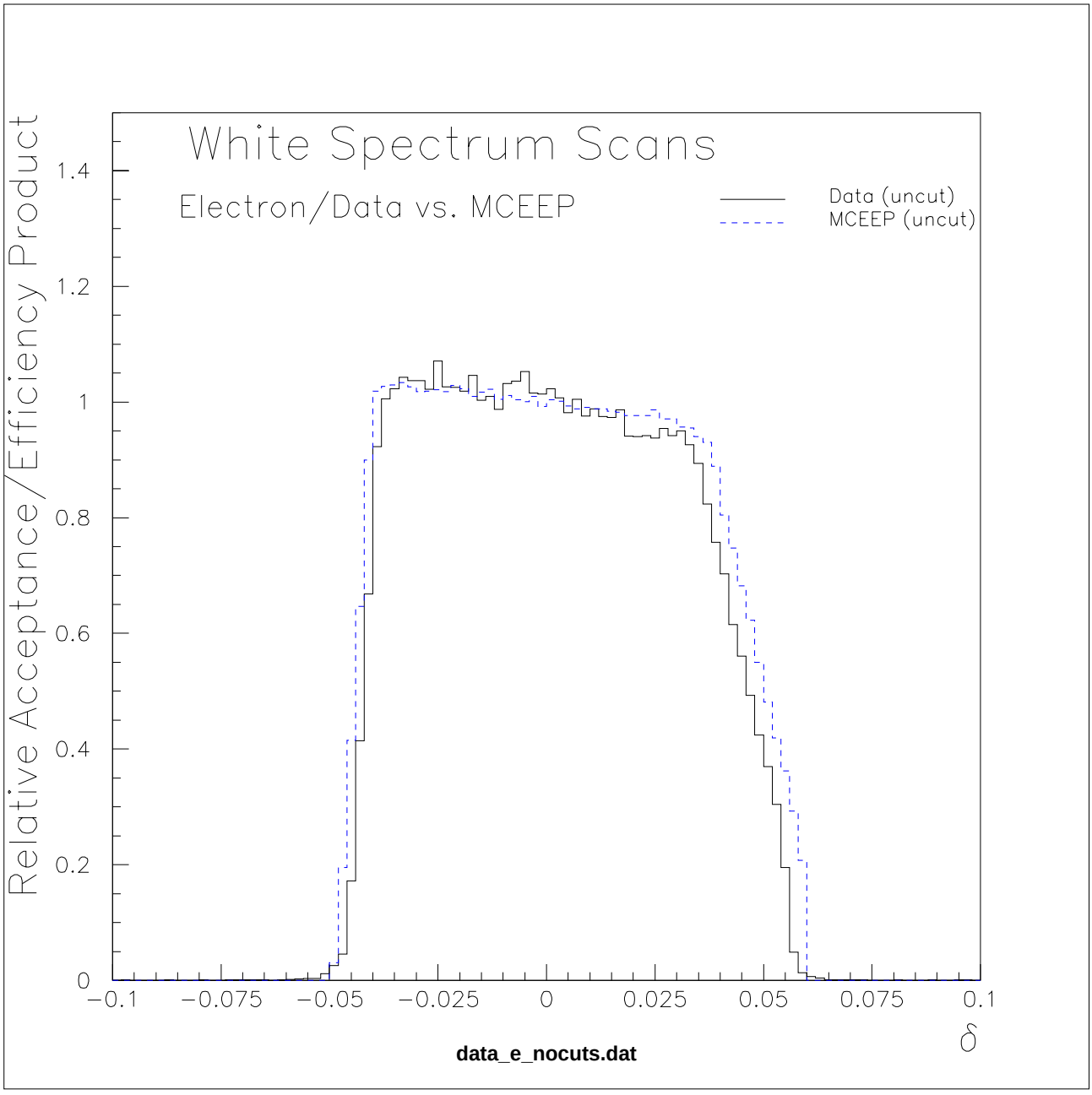

Figure 8: Electron arm relative acceptance/efficiency profile for data and for MCEEP. No acceptance cuts have been used, though the data are cut on the gas Čerenkov.

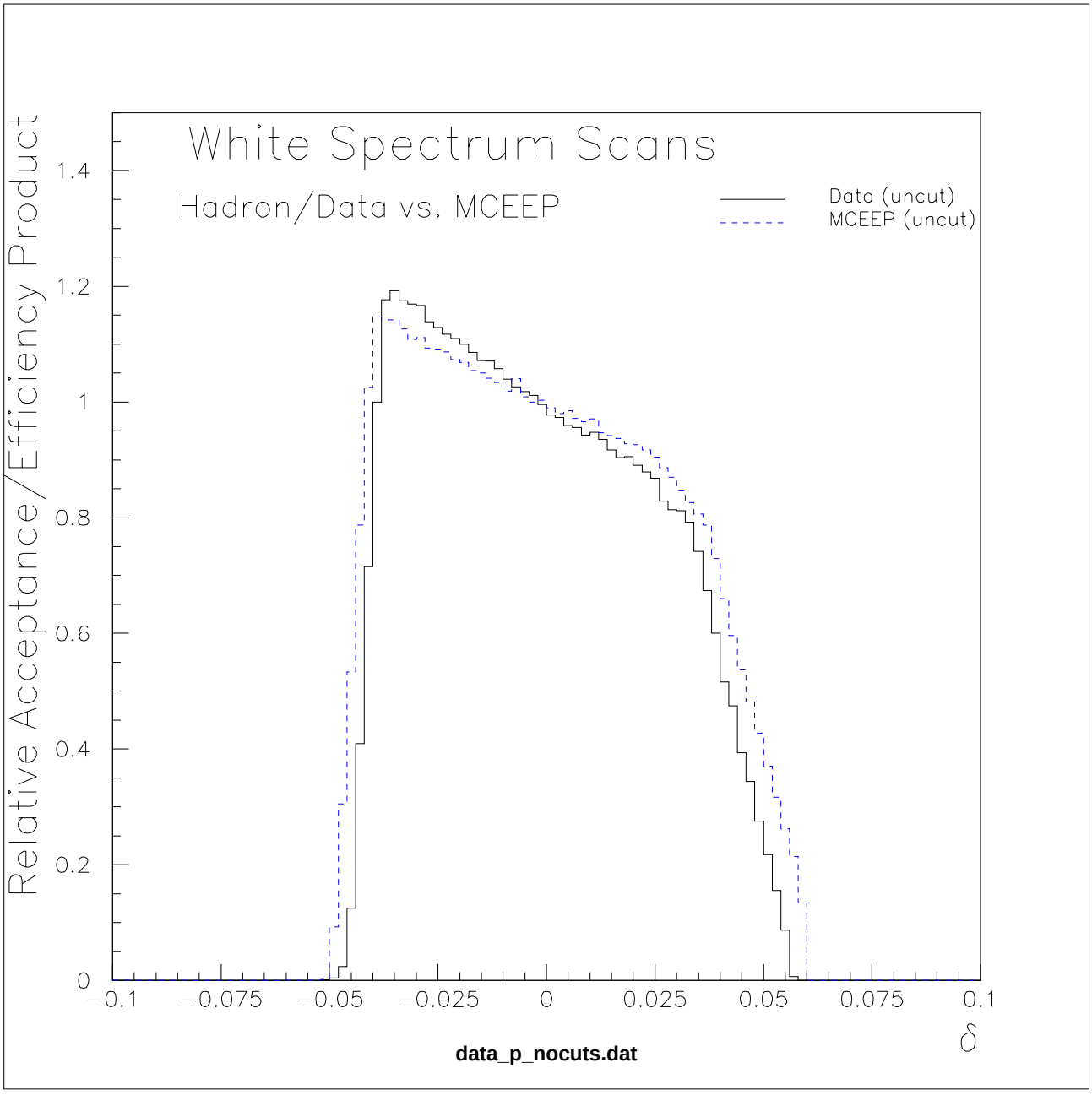

Figure 9: Hadron arm relative acceptance/efficiency profile for data and for MCEEP. No acceptance cuts have been used, though the data are cut on the 6.0 msr slit.

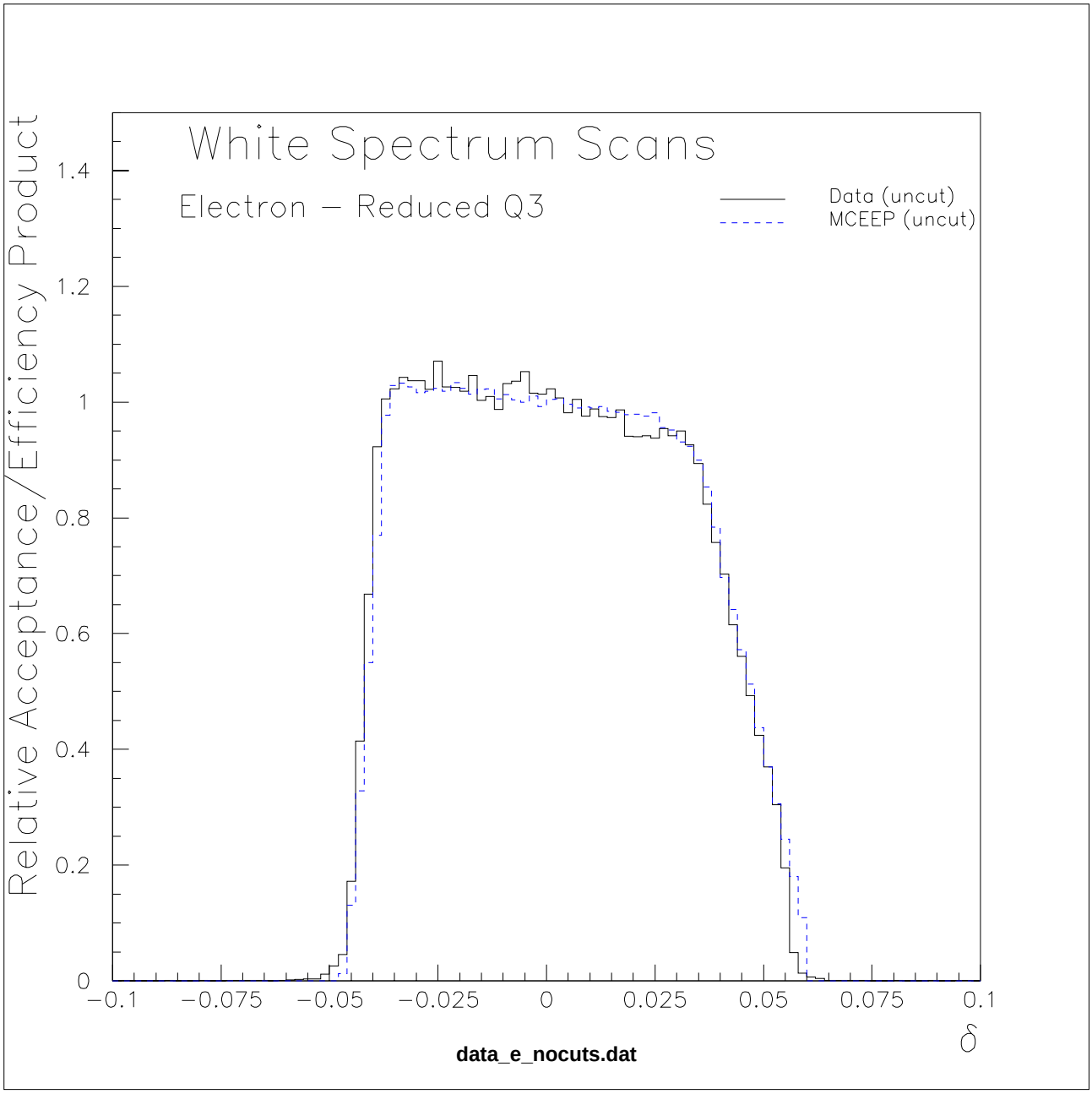

Figure 10: Electron arm relative acceptance/efficiency profile for data and for MCEEP using a reduced Q3 aperture of 0.28 m rather than the actual 0.30 m. No acceptance cuts have been used, though the data are cut on the gas Čerenkov.

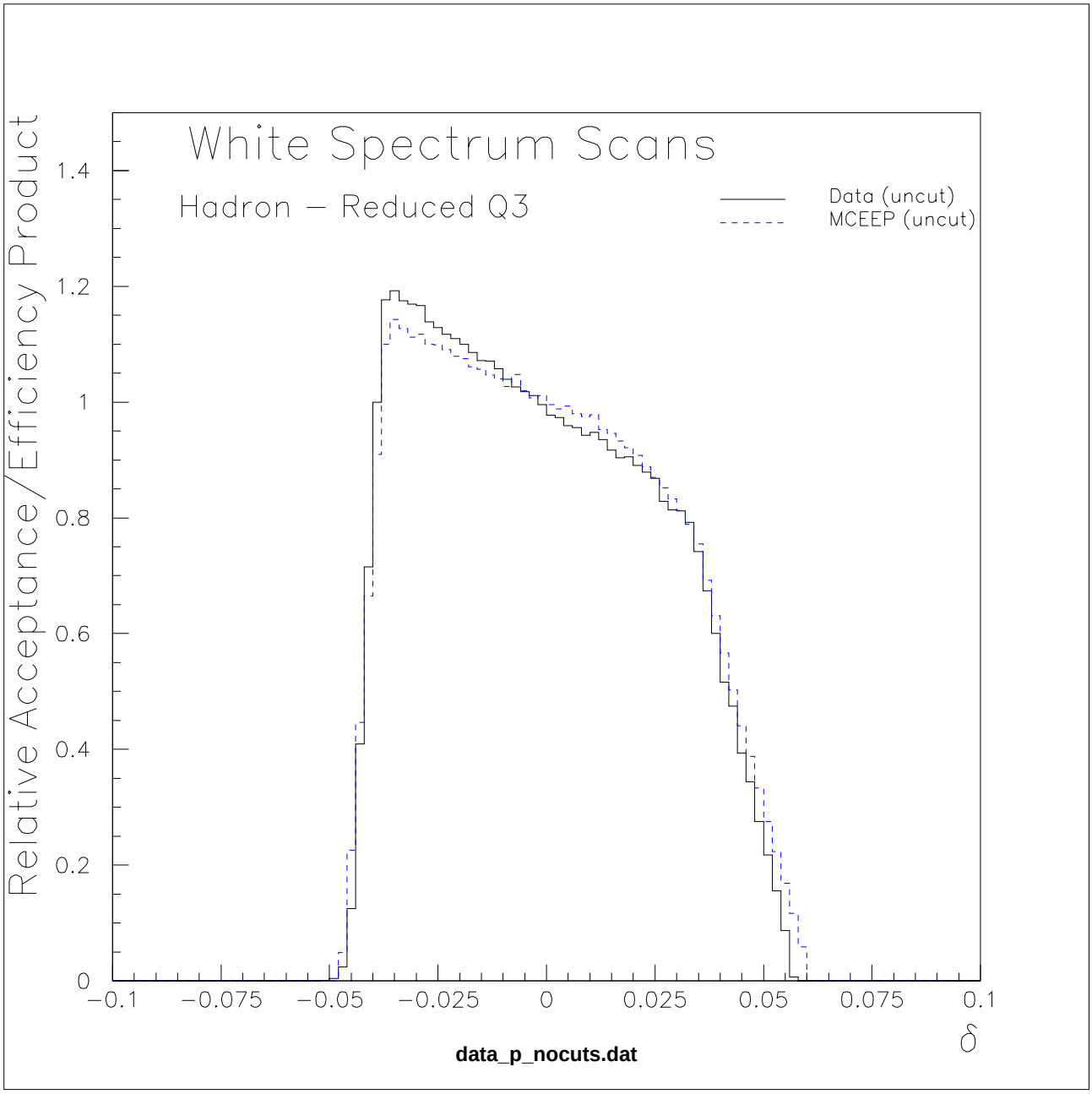

Figure 11: Hadron arm relative acceptance/efficiency profile for data and for MCEEP using a reduced Q3 aperture of 0.28 m rather than the actual 0.30 m. No acceptance cuts have been used, though the data are cut on the 6.0 msr slit.

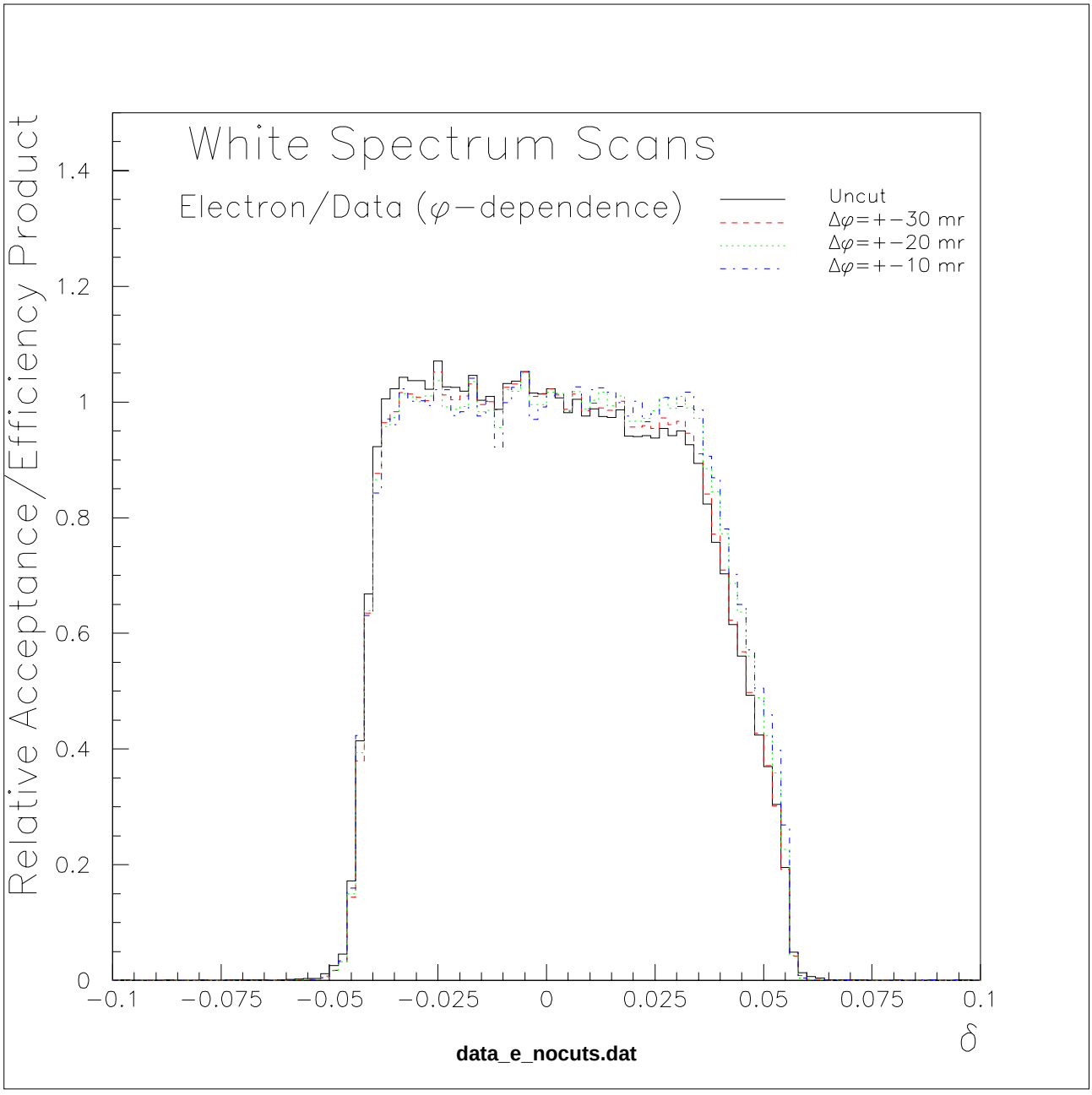

Figure 12: Electron arm relative acceptance/efficiency profile for data for various cuts on ϕ at the target. In each case the data have been cut on the gas Čerenkov.

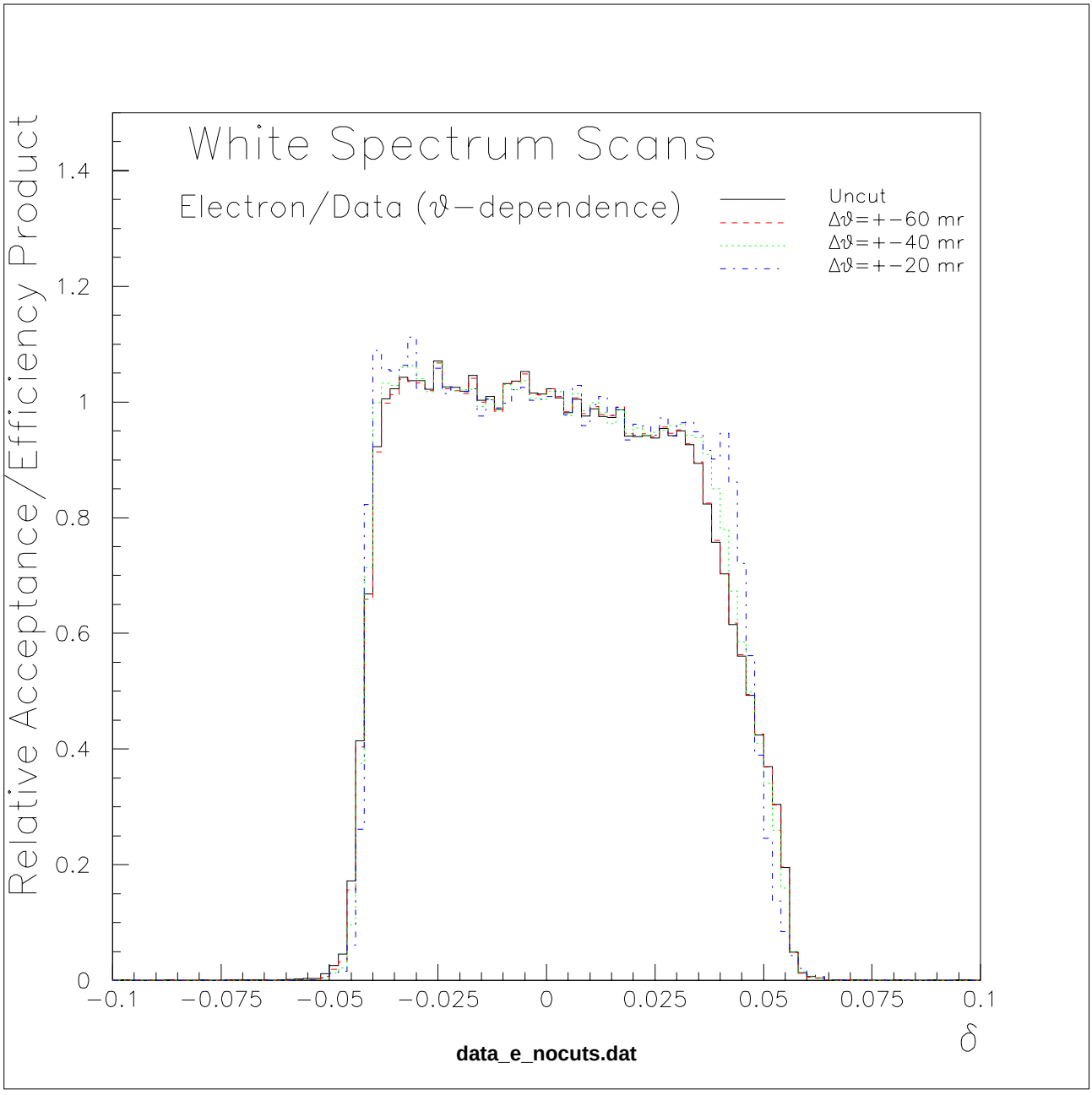

Figure 13: Electron arm relative acceptance/efficiency profile for data for various cuts on θ at the target. In each case the data have been cut on the gas Čerenkov.

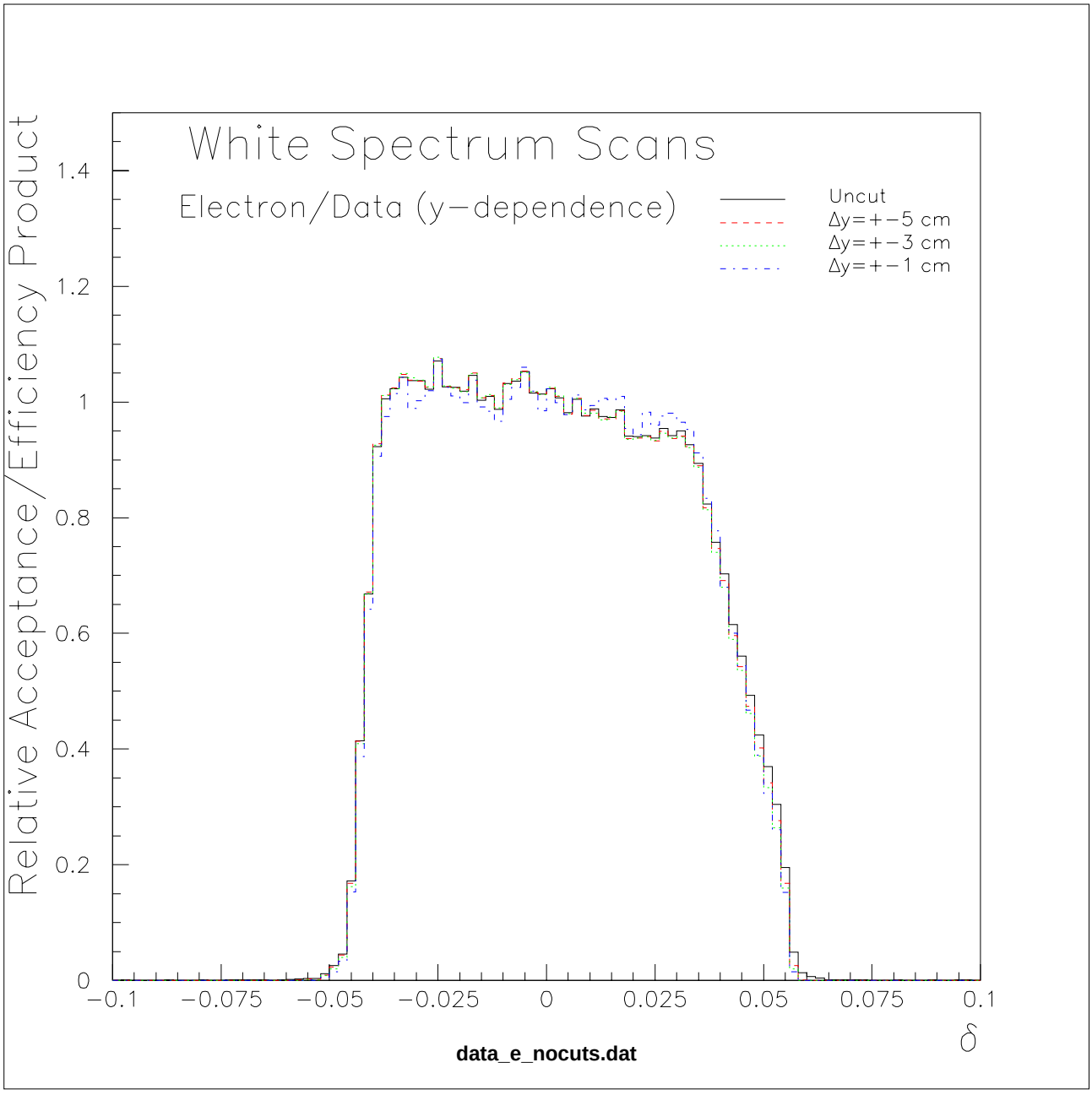

Figure 14: Electron arm relative acceptance/efficiency profile for data for various cuts on y at the target. In each case the data have been cut on the gas Čerenkov.

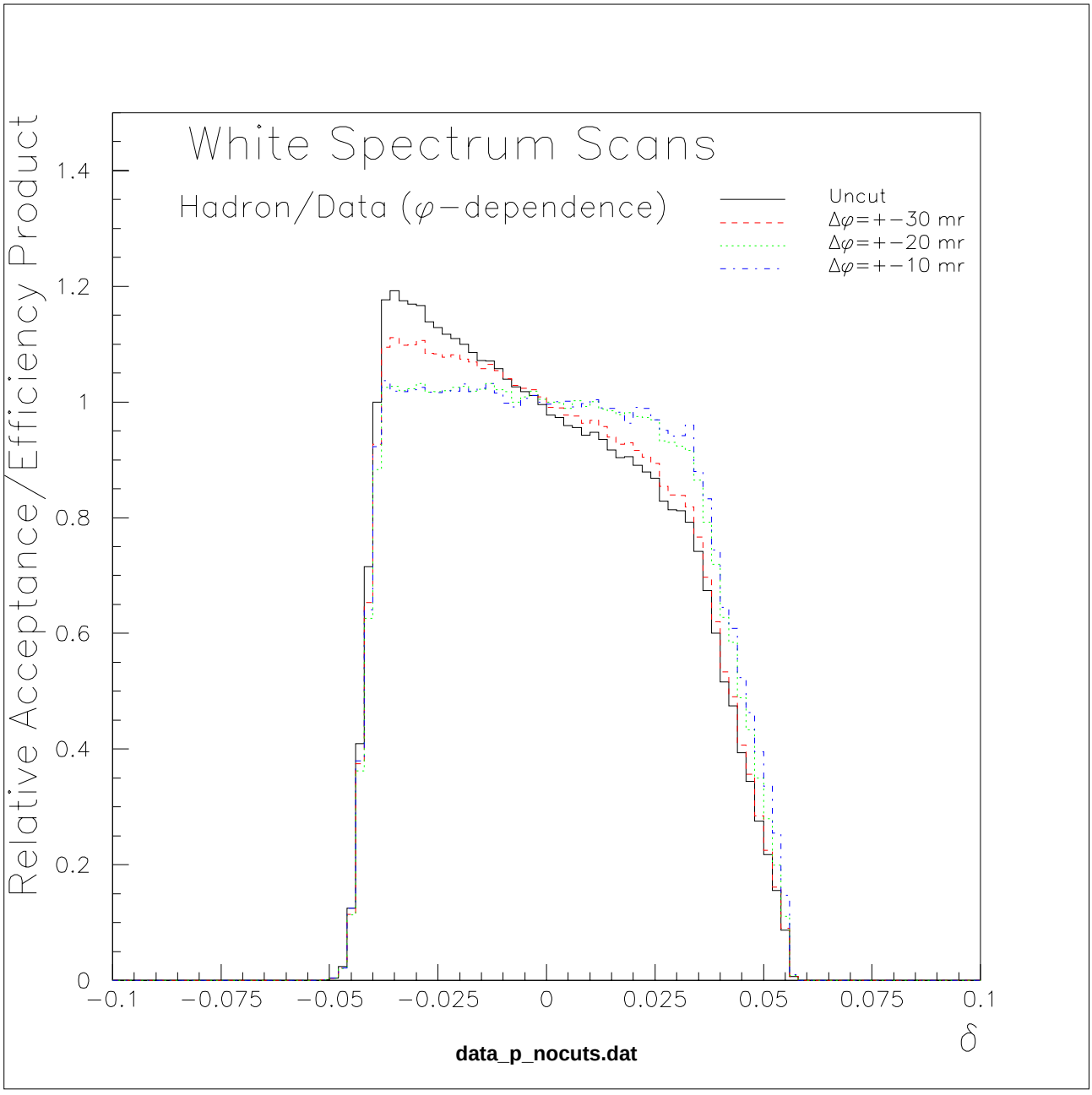

Figure 15: Hadron arm relative acceptance/efficiency profile for data for various cuts on ϕ at the target. In each case the data have been cut on 6.0 msr slit.

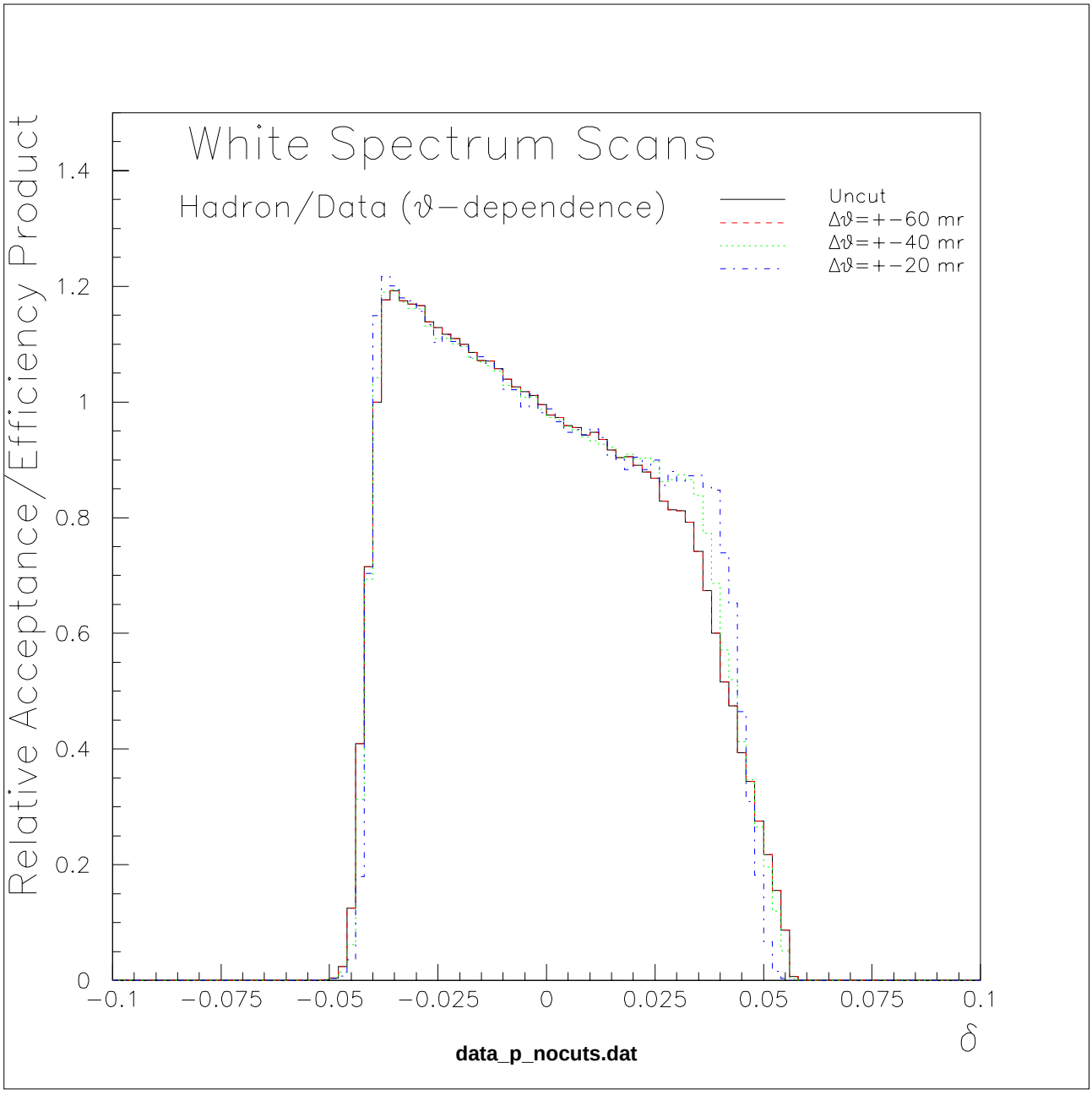

Figure 16: Hadron arm relative acceptance/efficiency profile for data for various cuts on θ at the target. In each case the data have been cut on 6.0 msr slit.

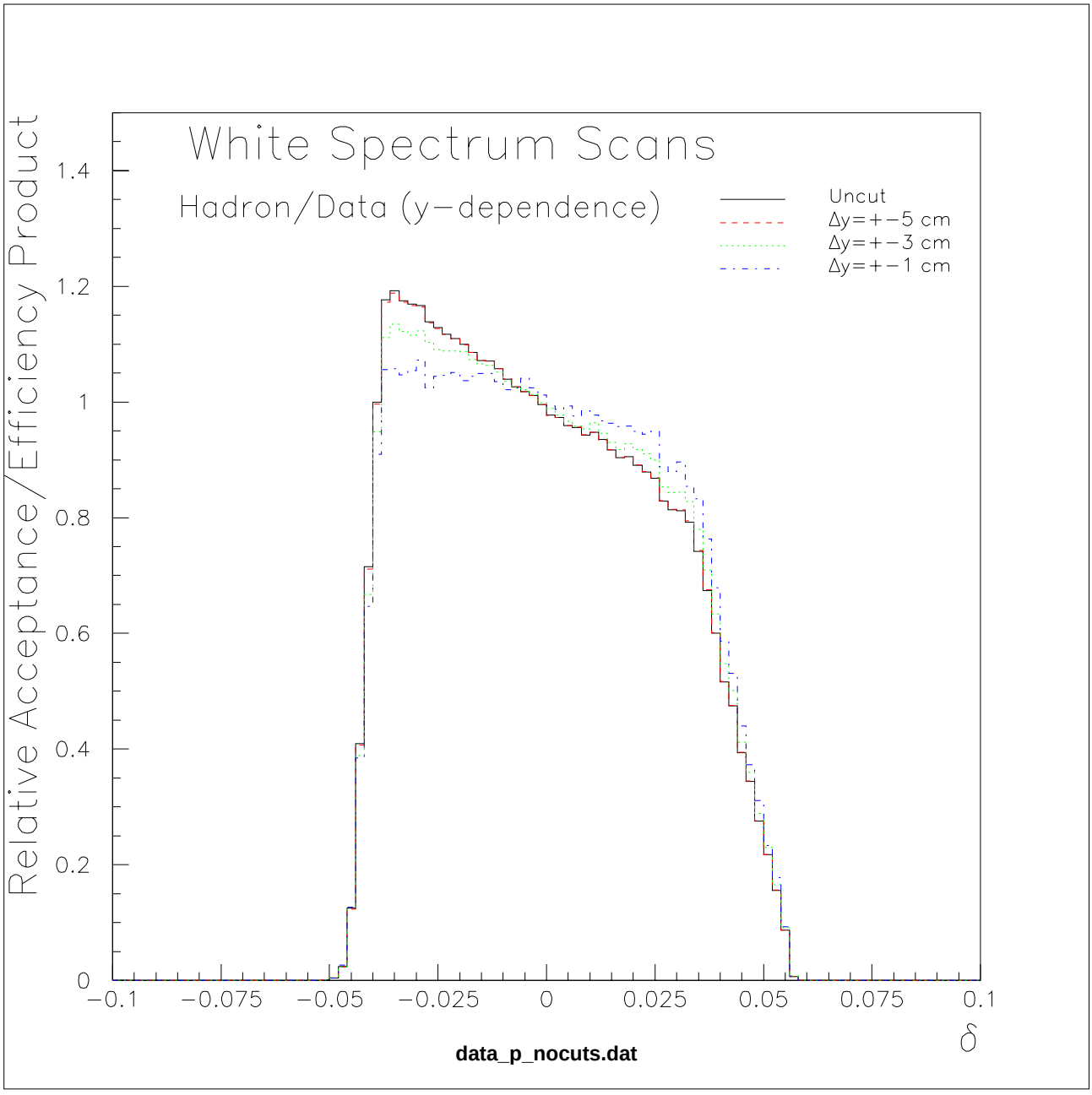

Figure 17: Hadron arm relative acceptance/efficiency profile for data for various cuts on y at the target. In each case the data have been cut on 6.0 msr slit.